Lawrence Berkeley Laboratory
UNIVERSITY OF CALIFORNIA

Accelerator & Fusion
Research Division

Presented at the 1988 European Particle Accelerator
Conference, Rome, Italy, June 7–11, 1988

Design and Fabrication of 33 GHz High-Gradient Accelerator Sections

D.B. Hopkins, A.M. Sessler, H.A. Johnsen,
J.C. Farmer, W.K. Kelley, C.P. Steffani,
J.Haimson, and B. Mecklenburg

June 1988

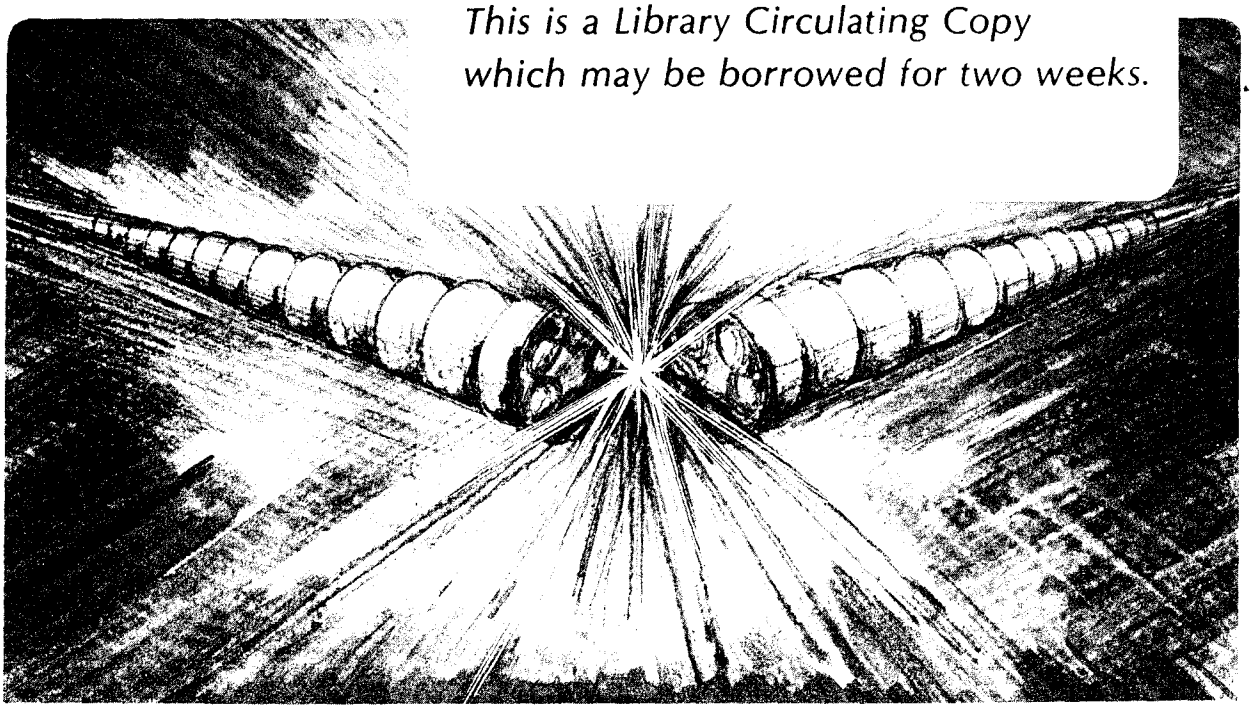

Prepared for the U.S. Department of Energy under Contract Number DE-AC03-76SF00098.

DESIGN AND FABRICATION OF 33 GHz HIGH-GRADIENT ACCELERATOR SECTIONS

D. B. Hopkins, and A. M. Sessler
Lawrence Berkeley Laboratory
Berkeley, Ca. 94720

J. C. Farmer, W. K. Kelley and C. P. Steffani
Lawrence Livermore National Laboratory
Livermore, Ca 94550

H. A. Johnsen
Sandia National Laboratory
Livermore, Ca. 94550

J . Haimson and B. Mecklenburg
Haimson Research Corporation
Palo Alto, Ca., 94303

This work was supported by the Office of Energy Research, High Energy Physics Division of the U.S. Department of Energy under Contract No. DE-AC03-76SF00098. Performed jointly under the auspices of the U.S. Dept. of Energy by LLNL under W-7505-ENG-48, and the Sandia National Lab., Livermore under DE-AC04-760P00789.

DESIGN AND FABRICATION OF 33 GHz HIGH-GRADIENT ACCELERATOR SECTIONS

D. B. Hopkins, and A. M. Sessler
Lawrence Berkeley Laboratory
Berkeley, Ca. 94720

J. C. Farmer, W. K. Kelley and C. P. Steffani
Lawrence Livermore National Laboratory
Livermore, Ca 94550

H. A. Johnsen
Sandia National Laboratory
Livermore, Ca. 94550

J . Haimson and B. Mecklenburg
Haimson Research Corporation
Palo Alto, Ca., 94303

Abstract

As part of a two-beam accelerator research program, ~33 GHz accelerator sections have been designed and fabricated by both the machined-and-brazed technique and the electroforming technique. These procedures are summarized in this paper. Special requirements included a filling time of about 14 ns, ± 1.25 μm dimensional tolerances, input VSWR ≤ 1.10, radial vacuum pumping for each cell, and a capability for a 200-300 MV/m accelerating gradient. A 34-cavity, $2\pi/3$ mode, quasi-constant gradient, $v_p=c$, ~ 10 cm - long, disc-loaded waveguide structure design was chosen with optimized sidewall input/output iris couplers

This work was supported by the Office of Energy Research, High Energy Physics Division of the U.S. Department of Energy under Contract No. DE-AC03-76SF00098. Performed jointly under the auspices of the U.S. Dept. of Energy by LLNL under W-7505-ENG-48, and the Sandia National Lab., Livermore under DE-AC04-760P00789.

Introduction

An initial goal of our two-beam accelerator (TBA) program has been to demonstrate the high accelerating gradients, e. g., 200 - 500 MV/M, which are feasible in disc-loaded waveguide structures at frequencies in the 35 GHz range.[1] An earlier seven-cavity copper test structure achieved an equivalent accelerating gradient of 180 MV/m during a 3.1 MW, 15 ns pulse at 34.6 GHz with only routine metallurgy and relatively poor vacuum involved.[2] Encouraged by this result, we began the construction of two identical high-quality, high-gradient accelerator (HGA) sections using different techniques. The first was fabricated using the machine-and-braze technique. The second was to employ the electroforming approach since it appeared that this method might significantly simplify the fabrication of these sections. Our intent was to comparison-test the two at high power to determine if either was superior to the other in achieving the desired high accelerating gradients. This paper reviews the requirements and design considerations for these accelerator sections and gives details of the techniques used in their construction. In so doing, it summarizes information presented elsewhere in greater detail.[3-5]

Design Considerations

The source of high 33 GHz microwave power available to us for testing structures was the LLNL ELF free-electron laser (FEL)[6]. Its operating pulse width and the center frequency of its tunable driver magnetron dictated that the fill-time and operating frequency of the accelerator structure be about 14 nsec and 33.3 GHz, respectively. A $2\pi/3$ mode, $v_p=c$, disc-loaded traveling wave structure was chosen for the HGA because the ratio of maximum surface field to average accelerating field could be maintained at less than 2.2. High gradient breakdown threshold data could be compared directly with previous RF breakdown experiments performed on similar geometry structures at lower frequency.[7] Also, accurate cavity, disc iris shaping and sidewall iris coupler design information was available from a wide variety of previously constructed research accelerators designed to operate at lower frequencies.

A constant-gradient design was initially chosen because of its many advantages.[8] However, the adoption of a strictly constant gradient design requires each disc iris aperture and each cavity diameter to be machined with different dimensions. Considering the extremely tight tolerances (±0.6 to 1.3 μm) associated with the critical dimensions of the 33 GHz cavities, batch machining with a minimum number of program changes to the CNC lathe and coordinate measuring inspection equipment was highly desirable to ensure acceptable yields and to

minimize costs. Thus, there is a distinct advantage in reducing the number of different cavity dimensions required for a given structure design. Our method for achieving this was to adopt a quasi-constant gradient design. This technique[9], previously used for a wide variety of medium energy, high peak RF power S-band linacs constructed for synchrotron injectors, pulse stretcher rings and high duty factor research facilities, makes use of a plurality of uniform $2\pi/3$ mode segments of increasing impedance, interconnected by matched transition regions. The uniform segment cavity dimensions, and the number of cavities per segment, are selected to satisfy specific field or high order mode requirements,[10] while the transition regions are arranged to minimize voltage reflections.

An additional concern influenced our choice. A strictly constant gradient design will always result in the maximum surface field occurring at the beginning of the structure because the ratio of this field to the average accelerating field decreases with reduced iris diameter. However, for the 33 GHz tests, it was considered desirable to have the maximum surface field occur approximately half way along the waveguide to increase the probability of demonstrating breakdown thresholds well within the body of the structure, without being limited by input coupler sparking. In satisfying the 33 GHz HGA test requirements, the surface and accelerating field gradients were maximized towards the center of the structure by a small impedance adjustment of the uniform segments. The final waveguide assembly comprised four uniform impedance segments having iris diameters of 2.6045, 2.4348, 2.3040 and 2.1692 mm respectively. Figure 1 shows details of the cavity design. Unlike the majority of linac designs the HGA test structure was not influenced by the need to satisfy a given beam-loading specification. Emphasis was placed on demonstrating the desired field gradient profile and filling time, T_F.

While the field gradient profile is determined by the relative values of the distributed iris diameters, it is the absolute values of these diameters that establish the individual cavity group velocities and, therefore, the overall filling time for a given length structure. The final set of iris diameters, scaled from previously compiled and empirically confirmed 9.5 GHz design data, was obtained by iterative computations to give a harmonic mean group velocity of 0.0245c (±.001c), i.e., T_F = 14 ns. Although the group velocity was expected to remain constant with accurate geometric scaling, the normal 3/2 frequency scaling law for voltage attenuation (I) was expected to become less valid with decreasing millimetric wavelengths because of the increasing difficulty of maintaining the micro-geometric relationship between the RF skin depth (δ= 0.35 mm at 35 GHz) and the surface texture, including grain boundary surface dislocations. It is interesting to note, for example, that with lathe-turned cavity components, the lay direction on all the internal surfaces are at right angles to the TM_{01} mode RF current paths. Thus, when designing practical millimetric structures, allowance for some additional degradation of Q and shunt impedance should be made, especially when scaling from 2856 MHz. Although diamond polishing procedures were used on the HGA disc apertures (and some disc surfaces), after scanning electron microscope (SEM) surface studies on a variety of

cavity samples, the S-band scaled design values for I were arbitrarily increased by an 8% factor.

From the above considerations, it was possible to establish an overall length for the structure and to select a range of group velocities consistent with the desired field gradient profile along the structure which met the filling time design objective of 14 ns. A total of 34 cavities were selected for the final test structure, giving an overall electrical length of 4080 degrees and a distance between input and output coupler midplanes of 99mm ($11\lambda_o$). For an input RF power of 100 MW, the average accelerating field (and maximum surface field) at Z=0, L/3, 2L/3, and L are designed to be 293.3 (648.1), 307.9 (667.5), 310.1 (661.3) and 292.3 (614) MV/m, respectively.

Machined and Brazed HGA

In order to demonstrate the best possible performance, emphasis was placed on metallurgical studies of the OFHC copper components, achieving and maintaining a high surface finish on the cavity walls, minimizing contamination - especially due to airborne particles - and on providing a high vacuum in the 10^{-8} to 10^{-9} Torr range. The latter was achieved by increasing the center line pumping conductance and by arranging for the overall test assembly, including oversized tapered rectangular waveguides and input and output ceramic RF windows, to be high temperature vacuum processed and sealed-off with attached sputter ion appendage pumps. The number of separate cavity components and brazed joints were minimized by machining cup shaped cavities (disc and spacer combined) with interlocking pilots to assist in stacking and accurately positioning the braze alloy. Unlike prior practice, however, the critical cavity dimensions were machined to tolerances of less than ±1.25 μm and with R_a surface finishes of approximately 0.05 μm. For the final machining operation, a CNC diamond turning lathe, designed for contoured micro-machining, was used with a single crystal natural diamond tool having a point radius of 25.4±2.5 μm. This tool was specially shaped with radial cutting edges, top rake and clearance angle to enable programmed contoured cuts to be made in one continuous movement along the flat surface of the disc and through the contoured small diameter aperture (refer to Figure 1).

For this waveguide, adoption of the quasi-constant gradient design resulted in a substantial reduction (from 34 to 10) of the number of different dimensional settings necessary to fabricate the precision contoured iris apertures required for the overall assembly. The poor pumping conductance along the beam centerline, due to the small disc apertures (~2.5 mm) and the sidewall iris coupling holes (~2.5 x 2.75 mm), was improved by machining radial pump-out holes[11] through the thick walls of the main body cavities and encasing the waveguide with a stainless steel vacuum jacket. Machining dimensions were determined by scaling, as well as by cold stack measurements, with allowance for anticipated brazing changes and the need for a very slight amount of compression tuning. Tuning recesses machined in the thick

wall of the cavity were designed to minimize degradation of the internal surface finish. After measurement acceptance and prior to final inspection, the aperture radii were polished to a high surface finish using 6 μm and 3 μm diamond polishing compound and exacting cleaning procedures, based on metallographic surface preparation techniques.

The overall accelerator waveguide comprised three brazed sub-stacks, i.e., the main body cavity numbers 8 through 28, and the input and output coupler and assemblies shown in Figure 2. The sub-stacks were brazed with 35Au/65Cu alloy (1030°C) using precision fixtures to maintain cavity concentricity and alignment to ±.2.54 μm. Pumping manifolds were connected from the vacuum jacket to the input and output beam drift tubes contiguous to the RF coupler blocks. Input and output RF feeds were designed to avoid flange connections and discontinuities in the high field region close to the accelerator couplers by combining matched $4\lambda_g$ long 90° E-bend tapered impedance transitions with $7\lambda g$ long linear taper sections in integrally machined and brazed overall assemblies. High peak RF power, oversize WR28 stainless steel RF/vacuum flanges were designed to accurately align and extrude the internal edges of the metal gasket to form high compression, smooth internal RF joints. The Kyle technique[12] was used to match and tune the coupler cavity sub-stacks. After brazing the E-bend transitions (and vacuum jacket and flanges) to the coupler sub-stacks using 50Au/50Cu alloy (990°C), all three sub-stacks were azimuthally and longitudinally aligned and final brazed using a precision jig assembly and Silcoro 60 alloy (865°C). A microwave measurement and nodal tuning procedure resulted in a phase accuracy of ± 2° for each cell.[4] Figure 3 shows a view of the accelerator waveguide prior to closing the surrounding cylindrical vacuum jacket. The final microwave parameters of the HGA are summarized in Table I.

TABLE I. FINAL MICROWAVE PARAMETERS

Total Number of $2\pi/3$ mode, $v_p = c$ Cavities	34
Resonant Frequency in Air at 23.1°C, 760.5 mm Hg & 68.7% RH	33.3760 GHz
Resonant Frequency in Vacuo at 23.1°C	33.3858 GHz
Phase Shift per Cavity	120 deg
Total Voltage Attenuation (t)	0.395 Np
Input Group Velocity	0.0324c
Output Group Velocity	0.0172c
Harmonic Mean Group Velocity	0.0237c
Phase Dispersion	5.15 deg/MHz
Filling Time	14.3 ns
Frequency/Temperature Dependence	–0.56 MHz/°C
Shunt Impedance Range	155-168 MΩ/m
Axial Accelerating Field (Maximum in Cavity No.. 21)	$31.0\sqrt{P_o(MW)}$ MV/m

Maximum Surface Electric Field
(Disc No. 11) $66.8\sqrt{P_o(MW)}$ MV/m

Sapphire windows were integrated into the accelerator test assembly to enable viewing (arc detection) along the beam centerline and in the tapered E-bend rectangular waveguide assembly connected to the input coupler. Additionally, a 0.1 mm-thick titanium window was installed at the electron beam output port to facilitate later measurements on accelerated electrons. All of the accelerator subassemblies were hydrogen furnace-brazed at temperatures in the range of 1040 to 860°C. After final microwave tuning and matching, the overall assembly was baked out at 250°C, sealed off and delivered under vacuum. It is being maintained at a vacuum level in the 10^{-9} Torr range while awaiting a high-power microwave source for testing. (The ELF facility was dismantled in March, 1987, to make way for the rebuilding of the ETA induction accelerator.)

Electroformed HGA

The electroforming method requires the machining of a disposable mandrel upon which copper is electrodeposited. The mandrel is then chemically etched out. Our goal was to produce an HGA having the same dimensions and mechanical tolerances as were achieved in the brazed unit described above. To ensure that the ELF tests would be comparing only the two accelerator sections and not just the input/output couplers, the couplers for this HGA were made indentical to those of the brazed structure. Moreover, each included five machined cavities in a brazed subassembly. These were to be joined to the HGA later by electroplating. The electroformed section described in this paper therefore has 24 cavities.

The required cylindrical mandrel has 25 slots of width 0.50089 mm, spaced by 2.4991 mm and cut to varying depths of approximately 3 mm. The rounded slot-root was permitted to be fully radiused, to simplify preparation of the cutting tool. Because of the limited usage necessary, a carbide tool was selected. The nose of the tool was precision-ground to a circular radius accurate to ± 0.48 μm and with a cutting-edge smoothness of < 0.076 μm (R_a). The common 6061-T6 aluminum alloy was used for the mandrels. We intended to microscopically inspect finished units for voids before plating them. The mandrels were machined at LLNL on a Pneumo precision T-base lathe which had an air-bearing spindle, vibration isolation system, laser feedback, and an Allen-Bradley computerized numerical control system capable of one-microinch resolution. During machining, the mandrel and chuck were bathed in temperature-regulated cutting fluid. The entire room was temperature regulated to < 0.1 °F. Details of the machining operation are given in reference 5. The initial acceptable part yield was poor. As problems were overcome, however, the yield increased to at least two "good" mandrels per day with perhaps one out-of-tolerance mandrel being produced every day or two. Nine good

mandrels were finally produced. We anticipated that the numerous possible pitfalls in handling and in subsequent electroforming steps might require several re-starts with new mandrels. The machining computer program was checked by carefully measuring the key diameters and spacings on test mandrels. Subsequent mandrels were first checked on an optical comparator, then precision-measured by a granite slab-mounted Laseruler[13] capable of one-microinch resolution and two-microinch repeatability. Optical interferometry was employed to confirm the three-microinch surface finish of the curved slot-root, the slot sidewalls, and the outer finished diameters. No final polishing of surfaces was planned since this might leave small, irregular particles embedded in the mandrel. These could, in turn, become embedded in the copper plating and reduce ultimate arcing thresholds. A finished mandrel is shown in Figure 4 along with three lucite masks, discussed below.

A variety of copper-plating studies was conducted[5] in a search for the best technique for achieving our requirements for (1) reliable deep-slot plating, (2) low porosity, inclusions and grain size, (3) precisely replicated mandrel surface, and (4) negligible void formation and outgassing at bakeout temperatures as high as 450°. We finally chose a cyanide copper bath which consisted of 64 gm/l copper cyanide, 112 gm/l sodium cyanide, and 19 gm/l sodium hydroxide. The organic additives were Allied Kelite Isobrite Nos. 625 and 630 at 3.1 and 0.5 vol. %, respectively. The part was rotated at 10 rpm. At an optimum dc plating current density of 21.5 A/m^2, a hyperfine, velvet grain structure developed which remained fine and randomly oriented even after a 650°C bakeout. Some outgassing studies were performed. Acid-copper electroforms produced significant outgassing of carbonaceous species. The cyanide-copper parts outgassed relatively little by comparison. Further tests are required to quantify these results. To avoid a "seam" at the periphery of each slot and possible trapped fluids, we decided to limit the slot-plating thickness to ~ 0.15 mm. This left a ~ 0.15 mm circumferential opening at each slot which would permit later cleaning, improving the vacuum environment. If no further plating were done, however, the electroform would be weak and flexible, like a long bellows, after the mandrel was chemically etched out. To provide the necessary strength, we electroformed three longitudinal strengthening ribs onto the plated mandrel. These were equally spaced in azimuth. Figure 5 shows a ribbed HGA, produced to demonstrate feasibility. In the final HGA, however, the rib width and radial thickness were to be larger. Microwave power loss considerations required the radial pumpout holes to be ≥ 2.8 mm long copper. Also, deep counterbored holes were required in the ribs to facilitate the microwave tuning of cavities. Thinned cavity wall regions thus produced would be intentionally deformed in the tuning process. The lucite masks shown in Fig. 4 were designed to produce the larger electroformed ribs.

Budget restrictions and the cessation of ELF operations forced the termination of this effort before the final HGA could be electroformed, joined to the input/output couplers, tuned and baked out. We believe that the most difficult, but achievable, remaining tasks were the joining of the electroform to the coupler subassemblies, with adequate dimensional control, and the thorough cleaning of the

final assembly. Comparing the two HGA fabrication techniques, it has now been demonstrated that a 33 GHz HGA can be machined, brazed, and tuned in a relatively straightforward manner. Moreover, these have the considerable advantage of using superior copper having low gas content so that they may be baked out at a temperature of 900°C. The resulting cleanliness and purity of critical copper surfaces might be difficult to match in an electroformed HGA and would likely permit higher ultimate gradients.

References

[1] D. B. Hopkins and R. W. Kuenning, "The Two-Beam Accelerator: Structure Studies and 35 GHz Experiments," IEEE Trans . Nucl. Sci., NS-32, 3476-3480, (1985).

[2] D. B. Hopkins, et. al., "High-Power 35 GHz Testing of a Free-Electron Laser and Two-Beam AcceleratorStructures," Proc. of S.P.I.E. High-Intensity Laser Processes Conf., 664 , 61-73, Quebec City, Canada, (1986).

[3] D. B. Hopkins, et al., "Fabrication and 35 GHz Testing of Key Two-Beam Accelerator Components," Proc. Part. Accel. Conf., IEEE Cat. No. 87CH2387-9, pp. 80-82, March (1987).

[4] J. Haimson and B. Mecklenburg, "Design and Construction of a 33 GHz Brazed Accelerator Waveguide For High-Gradient Operation," Proc. Part. Accel. Conf., IEEE Cat. NO. 87CH2387-9, pp. 1928-1930, March (1987).

[5] D. B. Hopkins, et al., "Electroforming Process Development for a 33 GHz High Gradient Accelerator," Proc. Part Accel. Conf., IEEE Cat. No. 87CH2387-9, pp. 1815-1817, March (1987).

[6] T. J. Orzechowski, et al, in Free Electron Generators of Coherent Radiation, C. A. Brau, S. F. Jacobs, M. O. Scully, editors (SPIE, Bellingham, WA, 1983), p. 65.

[7] J. W. Wang and G. A. Loew, IEEE Trans. Nucl. Sci. NS-32, 2915, October 1985.

[8] R. B. Neal, editor, The Stanford Two-Mile Accelerator, W. A. Benjamin, Inc. (1968), Chap 6.

[9] J. Haimson, IEEE Trans. Nucl. Sci. NS-12, pp. 457, 505, and 996, June (1965.)

[10] Linear Accelerators, Eds. P. Lapostolle and A. Septier,. pp. 445 and 450, North Holland Publishing Co., Amsterdam, 1970.

[11] Ibid, pp. 277 and 420.

[12] Ibid, p. 293.

[13] Manufactured by Tropel International, a Division of GCA Corporation.

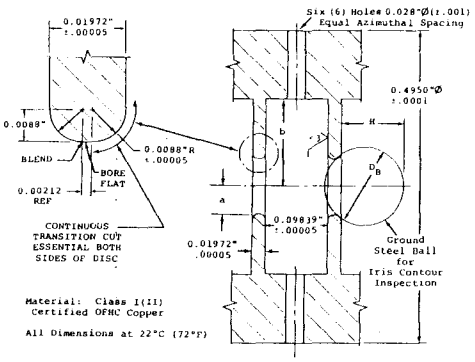

Fig 1. Cavity Design Details

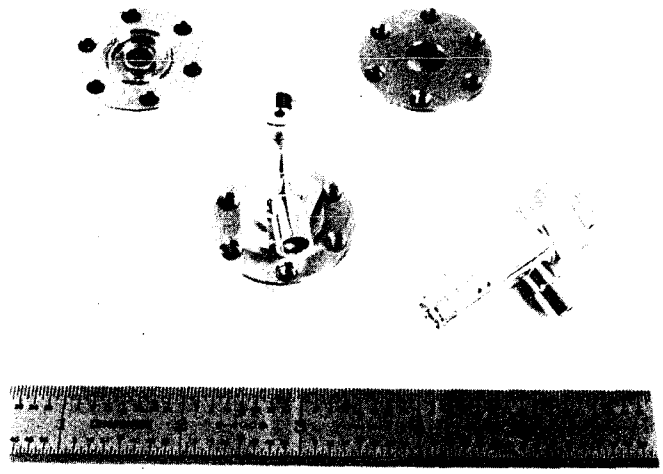

Fig 2. Input and Output Coupler Brazed Sub-Assemblies

CBB 872-1458

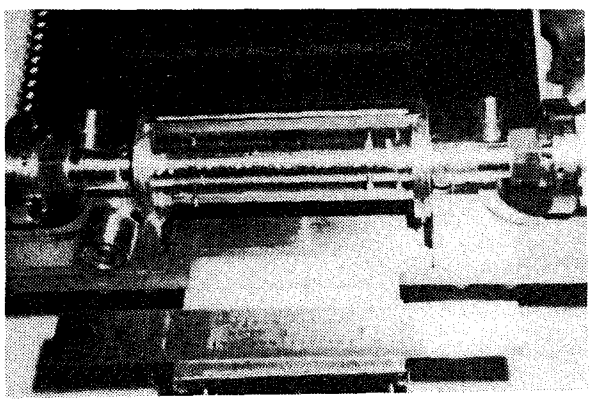

Fig 3. Accelerator Section Inside Vacuum Jacket

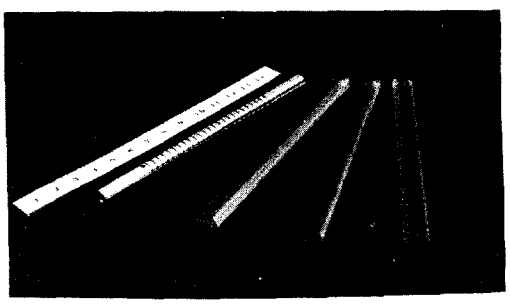

Fig 4 Mandrel and Lucite Masks

CBB 872-1310

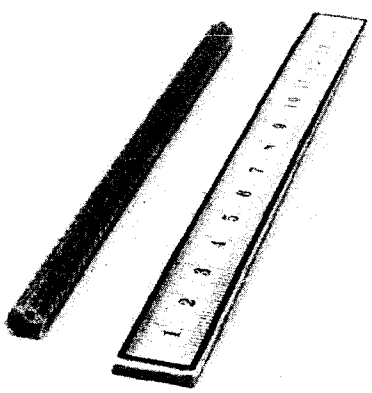

Fig. 5 Ribbed HGA Protype

CBB 866-4779

Lawrence Berkeley Laboratory
UNIVERSITY OF CALIFORNIA

Accelerator & Fusion
Research Division

Published in the Proceedings of the Orsay Workshop on
New Developments in Particle Acceleration Techniques,
Orsay, France, June 29–July 4, 1987

Phase Control of the Microwave Radiation in Free Electron Laser Two-Beam Accelerator

Y. Goren and A.M. Sessler

July 1987

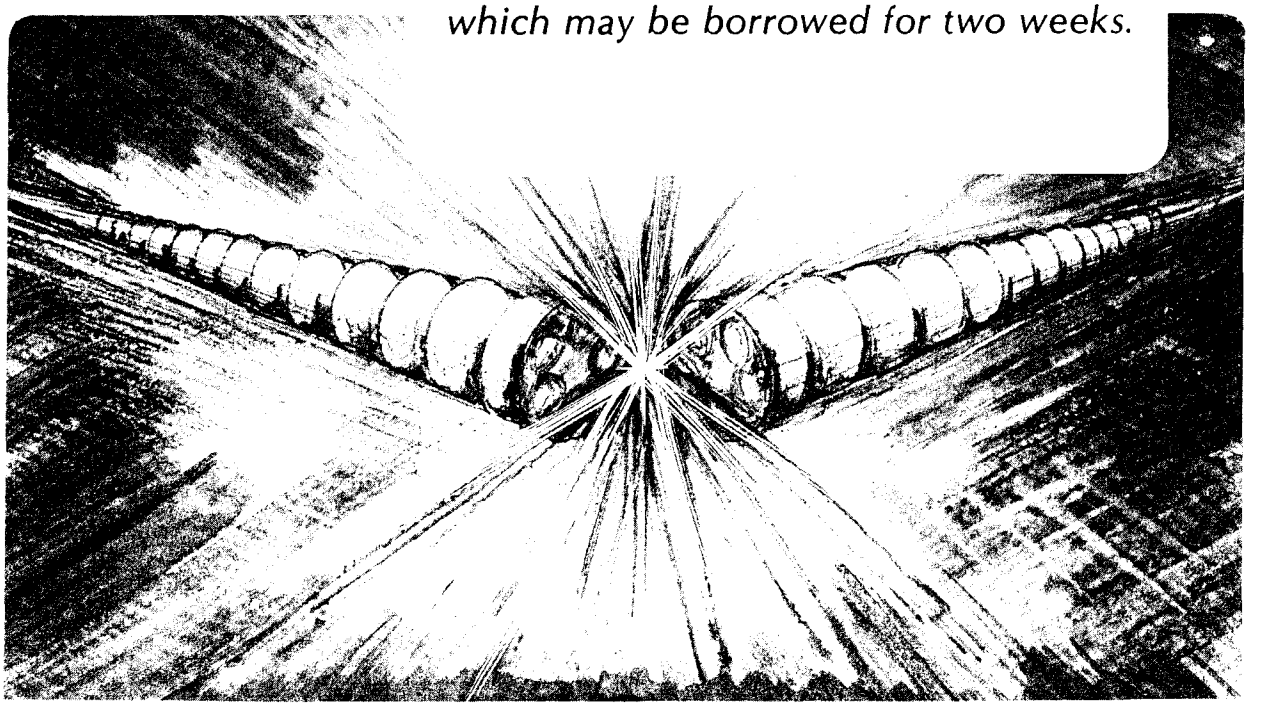

Prepared for the U.S. Department of Energy under Contract DE-AC03-76SF00098

PHASE CONTROL OF THE MICROWAVE RADIATION IN FREE ELECTRON LASER TWO-BEAM ACCELERATOR

Y. Goren and A.M. Sessler
Lawrence Berkeley Laboratory, University of California, Berkeley, CA 94720

Abstract

A phase control system for the F.E.L. portion of Two-Beam Accelerator is proposed. The control keeps the phase error within acceptable bounds. The control mechanism is analyzed, both analytically in a "resonant particle" approximation and numerically in a multi-particle simulation code. Sensitivity of phase errors to the F.E.L. parameters has been noticed.

1. INTRODUCTION

The two beam accelerator (T.B.A.) which utilizes the free electron laser (F.E.L.) has been proposed for future high gradient linear colliders.[1] To operate the T.B.A. a tight electro-magnetic phase control in its F.E.L. portion is needed.[2,3] Phase deviation results from accumulating errors in the F.E.L. section. Error sources are continuous current loss, wiggler field inaccuracy, or spatial fluctuation of the accelerating voltages across the induction units. Of particular concern is phase deviation resulting from shot-to-shot jitter in current, magnetic wigglers, and accelerating voltages. In this paper we propose a solution to the phase error caused by shot-to-shot jitter, via a "phase injection" mechanism. In this mechanism a number of correction stations will be spaced along the F.E.L. drift tube. At each station the microwave power flow will be replaced with microwave radiation of the same intensity, but with the phase expected from an ideal run (Fig. 1). In Section 2 we represent an analytical solution in the resonant particle approximation. A multi-particle numerical analysis is given in Section 3. In this section the results for phase error evolution from 1000 particles 1-D F.E.L. code will be presented and compared with the analytical results.

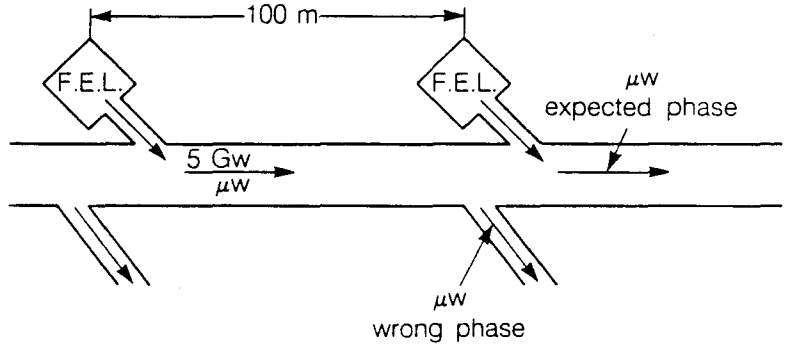

Fig. 1 Conceptual configuration of the phase injection system.

2. PHASE INJECTION IN THE RESONANT PARTICLE APPROXIMATION

To make the analysis easily understandable we shall treat the phase control mechanism only in the case of a current jitter. The same procedure applies in the other cases of fluctuations in the physical parameters. We shall use the resonant particle approximation with the standard K.M.S. notations.[4,5] The equations of motion are:

$$\frac{d\psi}{dZ} = k_w - \frac{w}{2\gamma^2 c}\,(1 + a_w^2 - 2a_w \cdot a_s \cos\psi) + \frac{d\phi}{dZ} \quad , \tag{1}$$

$$\frac{d\gamma}{dZ} = -w \cdot \frac{a_w \cdot a_s}{\gamma \cdot c} \sin\psi + \Delta' \quad , \tag{2}$$

$$\frac{da_s}{dZ} = \frac{1}{2}\,\frac{w_p^2\, a_w}{w \cdot c}\,\frac{\sin\psi}{\gamma} - \alpha a_s \quad , \tag{3}$$

$$\frac{d\phi}{dZ} = \frac{1}{2}\,\frac{w_p^2\, a_w}{w \cdot c\; a_s}\,\frac{\cos\psi}{\gamma} \quad , \tag{4}$$

where continuous acceleration, Δ', is assumed. The quantity Δ' is related to the microwave power extracted α through energy conservation:

$$\Delta' = \alpha \cdot \frac{2w^2\, a_s^2}{w_p^2} \quad . \tag{5}$$

With periodic replacement of the microwave radiation with radiation of the expected phase (phase injection) Eq. (4) should be changed into:

$$\frac{d\phi}{dZ} = \frac{1}{2}\,\frac{w_p^2\, a_w}{w\, c\, a_s} \cdot \frac{\cos\psi}{\gamma} + \sum_{M=1}^{N} (\Delta\phi_M) \cdot \delta(Z - M \cdot L) \quad , \tag{6}$$

where $\Delta\phi_M$ is the phase deviation at the M-th port and we assume in this analysis that all connected stations are equally spaced with a distance L between successive parts. The equilibrium condition (ideal run) is given by:

$$a_{s_0} = \frac{1}{2}\,\frac{w_p^2\, a_w}{\alpha \cdot w \cdot c}\,\frac{\sin\psi_0}{\gamma_0} \quad , \tag{7}$$

$$\phi_0' = \frac{d\phi_0}{dZ} = \frac{1}{2}\,\frac{w_p^2\, a_w}{w \cdot c\; a_{s_0}} \cdot \frac{\cos\psi_0}{\gamma_0} \quad ,$$

$$k_w - \frac{w}{2\gamma_0^2 c}\,(1 + a_w^2 - 2a_w \cdot a_{s_0} \cdot \cos\psi_0) + \frac{d\phi_0}{dZ} = 0 \quad ,$$

$$\Delta' = \frac{w \cdot a_w \cdot a_{s_0}}{c} \cdot \frac{\sin\psi_0}{\gamma_0} \quad .$$

We now study phase errors by assuming a small change from equilibrium originating from a small deviation $\zeta = -\frac{\Delta I}{I_0}$ in the injected current. Expanding all dynamical variables in ζ, we may write:

$$\psi = \psi_0 + \zeta\psi_1 + \zeta^2\cdot\psi_2 + \ldots \quad , \tag{8}$$

$$\gamma = \gamma_0 + \zeta\cdot\gamma_1 + \zeta^2\cdot\gamma_2 + \ldots \quad ,$$

$$a_s = a_{s_0} + \zeta\cdot a_1 + \zeta^2\cdot a_2 + \ldots \quad ,$$

$$\phi = \phi_0 + \zeta\cdot\phi_1 + \zeta^2\cdot\phi_2 + \ldots \quad .$$

To first order in ζ, we obtain four linear equations:

$$\frac{d\psi_1}{dZ} = -\frac{w}{2c\gamma_0^2}\left\{ -2\delta_1\cdot U_0 + 2a_w\cdot a_{s_0}\sin\psi_0\psi_1 - 2a_w\cdot\cos\psi_0\cdot a_1 \right\} + \tag{9}$$

$$+ \frac{d\phi_1}{dZ} \quad ,$$

$$\frac{d\gamma_1}{dZ} = -w\,\frac{a_w}{c\gamma_0}\left\{ a_1\cdot\sin\psi_0 - \delta_1 a_{s_0}\cdot\sin\psi_0 + \psi_1 a_{s_0}\cdot\cos\psi_0 \right\} \quad , \tag{10}$$

$$\frac{da_1}{dZ} = \frac{1}{2}\,\frac{a_w\cdot w_p^2}{w\cdot c\cdot\gamma_0}\left\{ -\sin\psi_0 \cdot \delta_1\sin\psi_0 + \psi_1\cos\psi_0 \right\} - \alpha a_1 \quad , \tag{11}$$

$$\frac{d\phi_1}{dZ} = \frac{1}{2}\,\frac{w_p^2\cdot a_w}{w\cdot c\gamma_0 a_{s_0}}\left\{ -\cos\psi_0 - \frac{a_1}{a_{s_0}}\cos\psi_0 - \delta_1\cos\psi_0 - \right. \tag{12}$$

$$\left. - \psi_1\sin\psi_0 \right\} + \sum_{M=1}^{N} \Delta\phi_{M(1)}\cdot\delta(Z-M\cdot L) \quad ,$$

where we use the notations:

$$U_0 = 1 + a_w^2 - 2a_w\cdot a_{s_0}\cdot\cos\psi_0 \quad ,$$

$$\delta_1 = \gamma_1/\gamma_0 \quad ,$$

and have assumed the following expansion for the phase deviation:

$$\Delta\phi_M = \zeta\cdot\Delta\phi_{M(1)} + \zeta^2\,\Delta\phi_{M(2)} + \ldots \quad . \tag{13}$$

The phase injected term in Eq. (12) acts as a periodic driving force initiating spatial oscillations of the dynamical variable. We expand the perturbated variables (Eqs. (9)-(12)) in a discrete Fourier expansion of the form:

$$\theta(Z) = \sum_{m=0}^{n-1} \theta_m \cdot \exp\left\{ i\, k_m \cdot Z \right\} \quad , \tag{14}$$

where $k_m = 2\pi \cdot M/L$,

$$\theta_m = \frac{1}{L} \int_0^L e^{-ik_m Z}\, \theta(Z)\, dZ \quad .$$

We obtain the four algebraic equations:

$$ik\,\psi_1 = 2\delta_1 U_0 \cdot \frac{w}{2c\gamma_0^2} - \psi_1 \frac{\Delta'}{\gamma_0} + \frac{a_1}{a_{s_0}} \cdot \frac{\Delta'}{\gamma_0} \cot\psi_0 + ik\phi_1 \quad , \tag{15}$$

$$ik \cdot \delta_1 = \frac{\Delta'}{\gamma_0} \left(- \frac{a_1}{a_{s_0}} + \delta_1 - \psi_1 \cdot \cot\psi_0 \right) \quad , \tag{16}$$

$$ik \cdot a_1 = \alpha a_{s_0} \left(-1 - \delta_1 + \psi_1 \cot\psi_0 \right) \quad , \tag{17}$$

$$ik\phi_1 = -\phi_0' \left(1 + \frac{a_1}{a_{s_0}} + \delta_1' + \psi_1 \cot\psi_0 \right) + \frac{\Delta\phi_{(1)}}{L} \quad , \tag{18}$$

where we drop the subscript "m" in the dynamical variables and the wave number k, and we assume the same phase deviation, to first order in ζ, in each section L. The solution for the electromagnetic phase shift ϕ_1 in terms of the equilibrium parameters is given from Eqs. (15)-(18):

$$\begin{aligned} ik_m \phi_{1m} \Bigg\{ & 1 - \frac{\alpha}{q_{am}} \cdot \frac{\phi_0'}{q_{\psi m}} \cot\psi_0 \left[1 - i \frac{\Delta'}{\gamma_0 q_{\gamma m}} \right] + \frac{\phi_0'}{q_{\psi m}} \frac{\Delta'}{\gamma_0 q_{\gamma m}} \cot\psi_0 \Bigg[1 - \\ & i \frac{\alpha}{q_{am}} \left(1 - iP_m \cdot \cot\psi_0 \right) \left(1 - i \frac{\Delta'}{\gamma_0 q_{\gamma m}} \right) \Bigg] - i \frac{\phi_0'}{q_{\psi m}} \tan\psi_0 \Bigg[1 - \\ & P_m \frac{\alpha}{q_{am}} \cot\psi_0 \left(1 - i \frac{\Delta'}{\gamma_0 q_{\gamma m}} \right) \Bigg] \Bigg\} = \\ & - \phi_0' \left\{ 1 + i \frac{\alpha}{q_{am}} - \frac{\Delta'}{\gamma_0 q_{\gamma m}} \cdot \frac{\alpha}{q_{am}} \left[1 - iP_m \cot\psi_0 \right] + P_m \tan\psi_0 \frac{\alpha}{q_{am}} \right\} + \\ & + \frac{\Delta\phi_{(1)}}{L} \end{aligned} \tag{19}$$

where we use the following notations:

$$iq_{\gamma m} = ik_m - \frac{\Delta'}{\gamma_0} \quad ,$$

$$iq_{\psi m} = ik_m + \frac{\Delta'}{\gamma_0} - i\,\frac{w}{c\gamma_0}\,\frac{U_0}{q_{\gamma m}} \cdot \frac{\Delta'}{\gamma_0} \cdot \cot\psi_0 \quad ,$$

$$iq_{am} = ik_m + \alpha + i\alpha a_{s_0}\,\frac{\Delta'}{\gamma_0 \cdot q_{\gamma m}}\,(1 - iP_m\cot\psi_0) + i\alpha\cot\psi_0 \cdot P_m \quad ,$$

and

$$P_m = \frac{\Delta'}{q_{\psi m}\gamma_0} \cdot \left[i\,\frac{w}{c\gamma_0}\,\frac{U_0}{q_{\gamma m}} + \cot\psi_0 \right] \quad .$$

For the zero oscillation mode, m = 0, the l.h.s. of Eq. (19) vanishes and we end up with an equation for the phase shift:

$$\Delta\phi_{(1)} = L\,\phi_0' \left\{ 1 + i\,\frac{\alpha}{q_{as}} - \frac{\Delta'}{\gamma_0 \cdot q_{\gamma_0}} \cdot \frac{\alpha}{q_{as}}\,[1 - iP_0\cot\psi_0] + \right. \tag{20}$$

$$\left. + P_0\tan\psi_0\,\frac{\alpha}{q_{a_0}} \right\} \quad .$$

In our parameter region (see Table 1) the wave numbers q_{a_0}, q_{γ_0}, q_{ψ_0} and the parameter P_0 can be approximated by:

$$q_{\gamma_0} \simeq i\,\frac{\Delta'}{\gamma_0} \quad , \quad q_{\psi_0} \simeq i\,\frac{w}{c\gamma_0}\,U_0\cot\psi_0 \quad , \tag{21}$$

$$q_{a_0} \simeq 2i\alpha \quad , \quad P_0 \simeq -i\,\tan\psi_0 \quad .$$

The average phase deviation, to first order in ζ, is given by substituting Eq. (21) in Eq. (20):

$$\Delta\bar{\zeta} = \zeta \cdot \Delta\phi_{(1)0} = \frac{1}{2}\,\zeta \cdot L\phi_0' \quad . \tag{22}$$

Hence the peak to peak phase oscillation is:

$$\Delta\phi_{pp} = 2\,\Delta\bar{\phi} = \zeta \cdot L\phi' \tag{23}$$

In the next section we present numerical results from a many particle simulation code. We shall see that analytical approximation given in Eq. (23) is in a good agreement with the numerical results.

3. MANY PARTICLE SIMULATION

In this section a many particle simulation code is used to study the behaviour of the electromagnetic phase in the phase injection scheme. Detailed description of the code is found in Ref. 6. The simulation uses discrete replenishment of the beam energy in the F.E.L. section. The code simulates the microwave propagation for different initial conditions and according to our phase injection scheme it replaces, at each correction station, the electromagnetic phase with the phase calculated from the optimum run.

In Fig. 2 we present the evolution of the phase error with distance along the F.E.L. drift tube, for the case of initial current deviation $\zeta = 0.13\%$ and without phase correction. The parameters of the run are given in Table 1. In Fig. 3 a phase injection has been applied at correct stations 60 m apart. One can see from the figure that the phase is confined in this case to $\Delta\phi_{pp} \leq 8.8°$. The analytical prediction for this set of parameters, given from Eq. (23), is $\Delta\phi_{pp} = 7.4°$. Each phase correction initiate a synchrotron oscillations, which results from the phase shift between the bunch center of gravity and the center of the potential well. The power extraction, represented by the parameter α in Eq. (3), tends to suppress these oscillations. We can see from the figure that after 3 to 4 e folds (15 to 20 m) the oscillations disappear and the phase deviation increases linearly with Z up to the next correction station.

Table 1

Parameters of the F.E.L. portion in two-beam accelerators

Average beam energy (units of mc^2)	40
Beam current	2.4 kA
Bunch length	6 m
Wiggler wavelength	27 cm
Peak wiggler field	3.2 kG
Average beam power	48 Gw
Power production	2.4 Gw/m

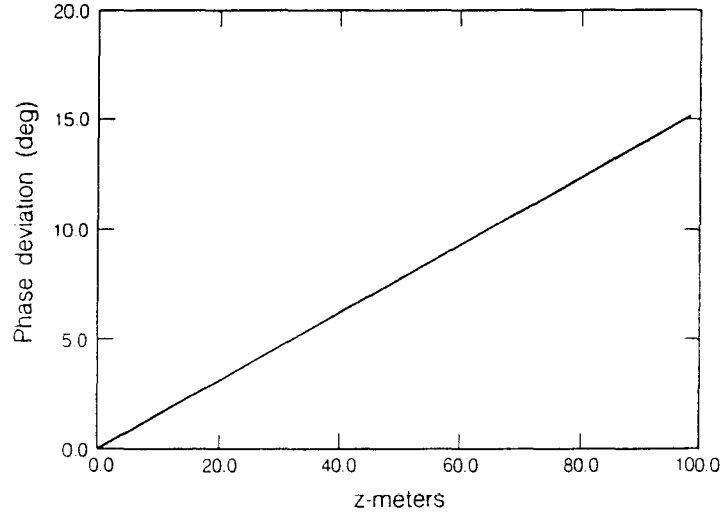

Fig. 2 Phase error vs. distance for 0.13% error in current $I_0 = 2.4$ kA.

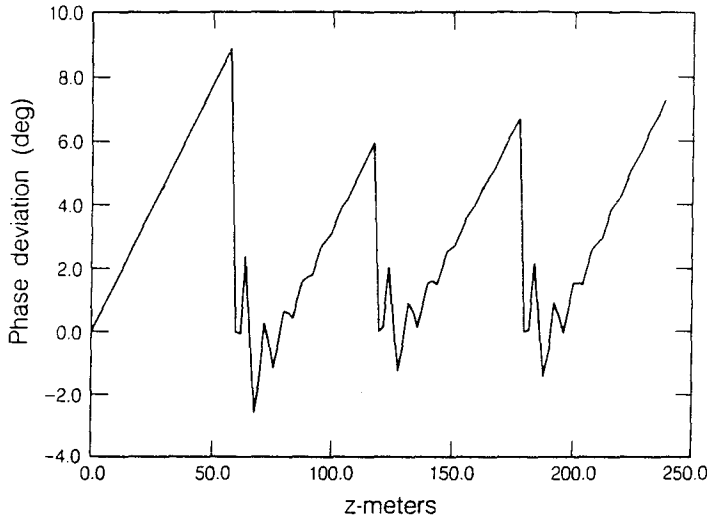

Fig. 3 Phase error vs. distance with phase injection stations 60 m apart.

To improve on this scheme we must increase the distance between correction stations without increasing the phase error. For this purpose we reduce the current flow from I_0 = 2.4 kA (see Table 1) to I_0 = 2.0 kA and the wiggler to 2.5 kG. In this mode of operation we could confine the phase error to $\Delta\phi_{pp} \leq 9°$ for 100 m between stations, and for the current deviation ζ = 0.13%. Figure 4 describes the phase vs. Z for this case. Thus we see that phase error is rather sensitive to TBA parameters, and since phase control is a central issue in a TBA perhaps parameters should be chosen with careful attention to phase control.

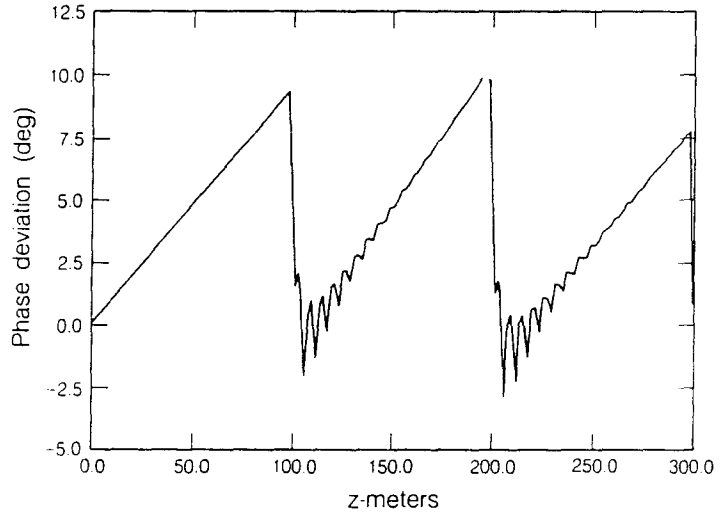

Fig. 4 Phase error vs. distance for 0.13% in current I_0 = 2 kA, and phase injection stations 100 m apart.

ACKNOWLEDGEMENT

This work was supported by the U.S. Department of Energy under Contract No. DE-AC03-76SF00098.

REFERENCES

1) A.M. Sessler, "The Free Electron Laser as a Power Source for a High Gradient Accelerating Structure," in Laser Acceleration of Particles, AIP Conf., Proc. No. 91, New York (1982); A.M. Sessler, IEEE Trans. on Nucl. Sci. NS-30 No. 4, 3145 (1983); A.M. Sessler, Proc. of the 12th Int. Conf. on High Energy Accelerators, Fermilab, p. 445 (1983).

2) R.W. Kuenning, "T.B.A. Phase Considerations," Lawrence Berkeley Laboratory Internal Report T.B.S. Note 12 (1984).

3) R.W. Kuenning, A.M. Sessler, and J.S. Wurtele, "Phase and Amplitude Considerations for the Two-Beam Accelerator." In Laser Acceleration of Particles II, AIP Conf. Proc., New York (1985).

4) N.M. Knoll, P.L. Morton, and M.W. Rosenbluth, IEEE Journal of Quantum Electronics QE-17, 1436 (1981).

5) R.W. Kuenning, A.M. Sessler, and E.J. Sternbach, "Radio Frequency Phase in the F.E.L. Section of a T.B.A.." In Symp. on Advance Accelerator Concept, Madison, WI, August (1986). LBL-22301

6) E.J. Sternbach and A.M. Sessler, "A Steady-State F.E.L.: Particle Dynamics in the F.E.L. Portion of a Two-Beam Accelerator." In Proc. of the 7th Int. Free-Electron Laser Conf., Tahoe City, CA. LBL-19939, September (1985).